IHJPAS. 37 (1) 2024
Ibn Al-Haitham Journal for Pure and Applied Sciences
Journal homepage: jih.uobaghdad.edu.iq
PISSN: 1609-4042, EISSN: 2521-3407

Comparison of the Optical Efficiency of Two Designs of the Maksutov–Cassegrain Telescope

[1]Marwa W. Abdulrahman **[2]Alaa B. Hasan*** **[3]Sameer H. R. Aldeen**

[1,2]Department of Physics, College of Education for Sciences Ibn-AL-Haitham, University of Baghdad, Baghdad, Iraq.
[3]Azarbaijan Shahid Madani University, Iran.

*Corresponding Author. alaa.b.h@ihcoedu.uobaghdad.edu.iq

Received: 7 February 2023, Received 24 February 2023, Accepted 13 March 2023, Published 20 January 2024

doi.org/10.30526/37.1.3276

Abstract

The research aims to develop the best possible design for the widely used Cassegrain telescope. The system consists of two models of different designs: (a) the telescope consists of a Maksutov lens, a spherical primary mirror, and a secondary mirror attached to the lens; (b) it consists of a Maksutov lens and a spherical primary mirror, plus a non-lens attached secondary mirror located between the lens and the primary mirror. The image was evaluated and analyzed using the analysis tools in Zemax software. The results of the two designs showed that the telescope whose secondary mirrors are not adjacent to the Maksutov lens produces high quality image that is almost free from aberration, and then comes the telescope whose secondary mirrors are adjacent to the Maksutov lens in terms of image quality. In the first design, the tangential and sagittal axes in the MTF function of the remaining angles (0.1, 0.2, 0.3, 0.4, and 0.5) contain two curves, which show how the loss of symmetry has changed the value of the function for the two axes. In the second design, the sagittal and tangential axes are identical in the angles of incidence (0, 0.1, and 0.2), and the transverse and sagittal axes of the remaining angles (0.3, 0.4, and 0.5) contain two curves. In PSF for the first design, there are several pretty high peaks on the surface of the image at the angle of incidence (0, 0.1). Since the shape is regular, the point spread function indicates that there isn't an aberration, but in terms of the angles (0.2, 0.3, 0.4, 0.5), we observe a gradual loss in intensity and the appearance of elevations on both sides of the picture. In the second design, at the angles (0, 0.1, 0.2, 0.3), we observe in Figure 5 that there are several high peaks free from aberration.

Keywords: Cassegrain telescope, Gregorian telescope, Rutten telescope, Zemax program, incidence angle.

This work is licensed under a Creative Commons Attribution 4.0 International License

1. Introduction

Cassegrain telescopes are optical telescopes made up of mirrors and lenses with specialized image-forming technology. The primary mirror of the Cassegrain telescope is a parabolic concave mirror, while the secondary mirror is spherical, with a focus that corresponds to the primary mirror's initial focus. Spherical aberration is not present in the surface's final image at secondary focus, but it is present in the off-axis photos. [1]

A mirror's spherical aberration is significantly less than that of a lens with an equivalent focal length, while a concave mirror's spherical aberration is the opposite when compared with a positive lens [2].

A spherical mirror and a negative meniscus lens make up the refracting Maksutov Cassegrain telescope. It is commonly known as a meniscus corrector lens when the negative lens is placed at the telescope's entrance. The advantage of this design is that it can rectify aberration issues like chromatic aberration and off-axis issues like coma in reflecting telescopes [3].

A small metal spot is presented on the inner face of the corrective lens in this form of Cassegrain design, also known as Gregory-Maksutov or Spot-Maksutov, which employs spherical surfaces. This facilitates fabrication and avoids the production of diffraction spikes in the presence of a (spider stent). These systems should have focal ratios higher than f/15 to prevent aberrations if all spherical surfaces are being utilized [4].

Additionally, because the secondary's radius is same as the posterior meniscus's radius, there is less flexibility in the optical system's correction when the secondary's radius is changed. In a second design, Gregory lessened aberrations by eliminating the spheres from the front corrector's (the main mirror) surface. [5]

Spherical aberration in a mirror is significantly smaller than in a lens with an equivalent focal length. Because the spherical aberration of the concave mirror is the reverse of that with respect to the positive lens, several studies have recommended employing a weak negative lens. In addition, two mirrors are needed for the Cassegrain system. The secondary mirror, which is smaller, is linked to the corrector lens, as the annular primary mirror has a central aperture [6].

These employ lenses, which significantly lower the physical length of the optical assembly, mostly by simulating a secondary convex mirror that will increase the focal length by a factor of (4 to 5 times). This results in lenses with focal lengths are substantially shorter and smaller than their long or telephoto equivalents, ranging from (250 mm) to (1000mm) [7]. Changes in the distance between the two mirrors has a significant impact on the telescope [8].

The primary mirror is annular concave, and once the rays are transferred there, it reflects them back to the front, where the secondary mirror is situated. The secondary mirror simulates a portion of the inner surface of the corrective lens by reflecting light onto the primary mirror's center, where it enters the eye lens and creates the picture [9].

2. Optical Design

The Maksutov-Cassegrain telescope consists of two mirrors and a passive crescent lens that collects light in the center. Maksutov-Cassegrain arrangements were made in three models: (a) a spherical correcting lens with an aluminum spot at the back of the corrector secondary (Gregorian pattern) with a spherical primary mirror as shown in **Figure (1-a); (b)** a spherical correction lens with a secondary mirror spaced to the rear of the lens with a primary spherical mirror as shown in **Figure (1-b).**

Tables 1 and 2 consist of the number of surfaces of the lens, mirrors, radius of curvature, thickness, types of glass, and semi-diameter calculated using the Zemax program (2013). So, from all the input data, we can see the design results as shown below.

Table 1. Lens data editor of Cassegrain design (Gregorian telescope) the correct lens attached to the secondary mirror

Surf :type		Radius	Thickness	Glass	Semi-Diameter	Conic
OBJ	Standard	Infinity	Infinity		Infinity	0
1	Standard	Infinity	30.000		0.000	0
2	Standard	Infinity	0.000		45.000	0
3	Standard	Infinity	-30.000		100.262	0
4	Standard	-334.956	20.000	BK7	120.000	0
5	Standard	-346.673	605.800		120.000	0
6	Standard	-1592.200	-605.000	MIRROR	120.000	0
7	Standard	-597.900	641.000	MIRROR	45.000	0
IMA	Standard	Infinity	-		21.531	0

Table 2. Lens data editor of Cassegrain design (Rutten telescope) the correct lens attached to the secondary mirror

Surf :type		Radius	Thickness	Glass	Semi-Diameter	Conic
OBJ	Standard	Infinity	Infinity		Infinity	0
1	Standard	Infinity	30.000		0.000	0
2	Standard	Infinity	0.000		45.000	0
3	Standard	Infinity	-30.000		100.262	0
4	Standard	-334.956	20.000	BK7	120.000	0
5	Standard	-346.673	605.800		120.000	0
6	Standard	-1592.200	-589.700	MIRROR	120.000	0
7	Standard	-598.072	832.100	MIRROR	45.000	0
IMA	Standard	Infinity	-		25.878	0

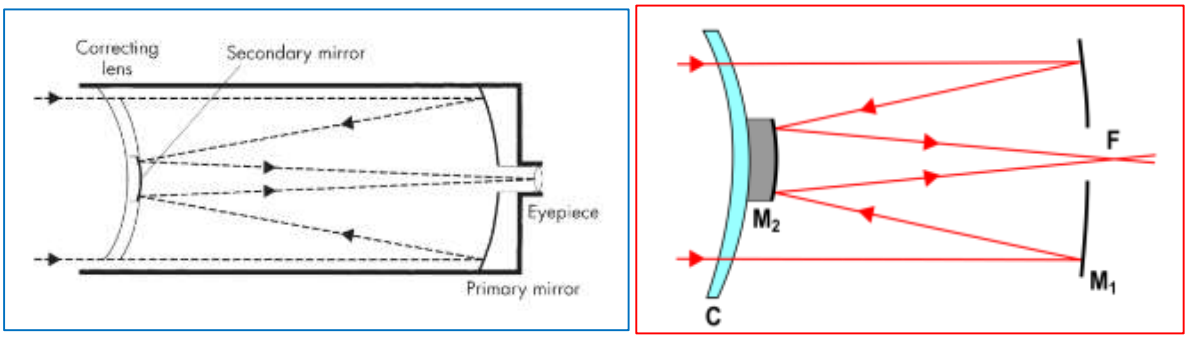

(A) **(B)**

Figure 1. (A) Maksutov Cassegrain telescope (Gregorian telescope) the correct lens attached to the secondary mirror. (B) Maksutov Cassegrain telescope (Rutten telescope) the correct lens nonattached to the secondary mirror [10] [11].

3. Evaluation Tools

Spot Diagram is a geometric illustration that gives a general notion of how the rays propagate geometrically in the image plane of an optical system [12]. It is a macroscopic approach of evaluation used to assess the image's quality. The good distribution of the image, which encircles an area (80%) of the overall distribution, may be compared using the Airy disk, which is the distribution area criterion. Only by evenly distributing the image throughout the Airy disk will the image be good [13].

Point Spread Function (PSF): The response of the imaging system to a point source is represented by the point spread function (PSF). The impulse response of a focused optical system is another

name for (PSF). PSF can be compared to the extended point in a picture that symbolizes a single-point object [14]. The imaging system's optical transmission function (PSF) is the spatial field version of this function. It is an important idea in the fields of astronomy, medicine, and other imaging methods like 3D microscopy [15].

Modulation Transfer Function (MTF) According to MTF, spatial frequency affects how much modulation is transferred from the object to the image. As an optimization and tolerance target during the lens design process, it is frequently used to define lens performance. The modulation transfer function (MTF) is a crucial tool for defining how well an optical system performs [16].

Optical Path Difference (OPD) is well known an effective way to gauge the effectiveness of an imaging system is the optical path difference (OPD). If the wave front that goes to an image of a point is spherical and focused in the bitmap of a specific field of view, the picture is fine, mathematically perfect, or diffraction-defined [17].

If the wave front is spherical, concentric, and concentrated at a place in the image, all rays will arrive at the same spot, which will be specified by the wave's center of curvature. The OPD of the curved surface wave will differ due to the curvature of the surfaces of mirrors and lenses, and this difference causes the rays to not gather after refraction or reflection at one point, which causes deflection [18].

Ray Fan Aberration (RFA) In order to give a notion of the sort of aberration occurring, the graphic for this function depicts how the rays are deflected from their original course in the sagittal plane and in a direction tangential to the optical axis. There are spherical aberration, chromatic aberration, comet, astigmatism, field curvature, and the amount of aberration in the optical system shown by the type, degree, and size of the aberration in the aberration curve [19].

Encircled Energy (Enc) Encircled energy optics are concentrate energy on the image plane. By first locating the central point and then dividing the image plane into concentric circular sectors that gradually move out from the center, PSF can be used to calculate the encircling energy of a point object. As the area of the circle grows, the total quantity of energy in the image plane rises until it is all contained [20].

4. Results and Discussion

4.1. Spot Diagram

Two different Cassegrain telescope designs were used, and an idea of the effect of the difference between them on the resolution and image quality was given by using Zemax optical analysis software.

To offer an understanding of the impact of varying the angle of incidence on the image quality, various values of the angle of incidence were employed. Due to the symmetry of the optical system and the two axes (y, x), the variable angle of incidence towards the x axis was only employed when using the field window in the Zemax program.

Figures (2 and 3) show the beam propagation plot in the image plane for three different designs of the Cassegrain telescope. With a difference in the angle of incidence, we observe a difference in the intensity distribution due to an aberration in the optical system caused by the object moving outside the optical axis.

In **Figure (2),** the rate of propagation of the rays increases gradually when the angle of incidence is greater than 0.2 at angles (0.3, 0.4, 0.5). Where the radius of the scattered rays at angle (0, 0.1, 0.2) is (6.614, 9.194, 13.133, µm), which is approximately identical to the standard Airy disk

whose value is (8.264 µm). As for the angles (0.3, 0.4, 0.5), the radii of the scattered rays (18.411, 25.023, 32.969 µm) are increased, and we note the direct proportionality of the angle of incidence with the value of aberration.

A separate secondary mirror is installed on the inner surface of the meniscus corrector in the Rutten Maksutov-Cassegrain. By adjusting the curvature of the corrector and the secondary separately, this offers an additional degree of flexibility in correcting aberrations. In particular, it enables the designer to aspherize the secondary to give a flat field that is significantly wider than that of conventional spot Maksutov and has a lower off-axis coma. The secondary being mounted on the corrector also reduces diffraction spikes.

In **Figure 3**, the rate of propagation of the rays is almost constant at the angles of incidence (0, 0.1, 0.2, 0.3). Where the radius of the rays scattered at those angles is (2.969, 2.341, 3.718, 7.357 µm), which is identical to the Airy disk standard, whose value is (9.943 µm), and the diameter of the rays spread increases at the angles (0.4, 0.5), where its value is (12.599, 19.555 µm), respectively. We also note the direct proportionality of the angle of incidence with the value of deviation.

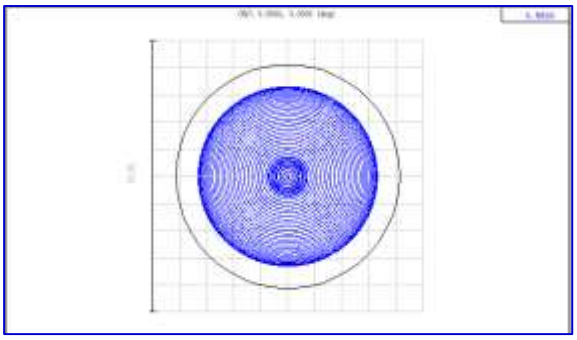

(A)

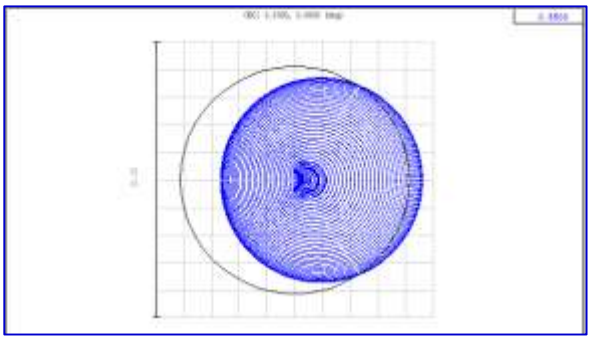

(B)

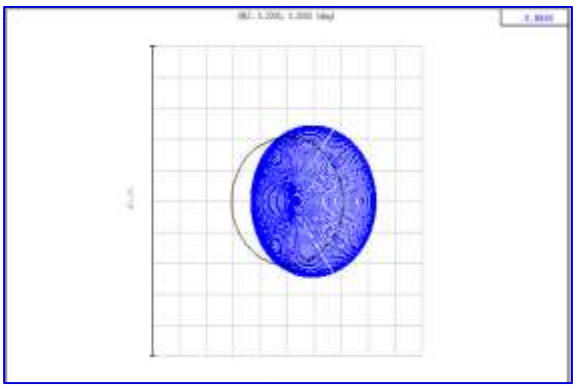

(C)

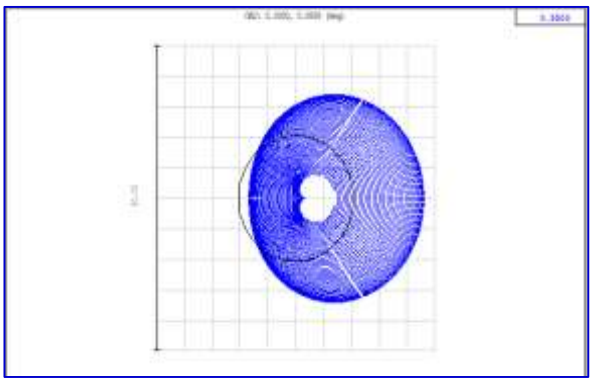

(D)

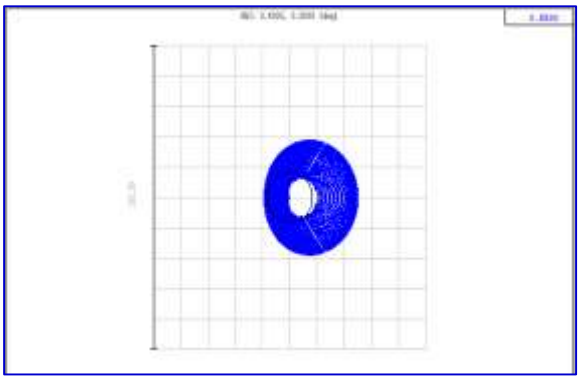

(E)

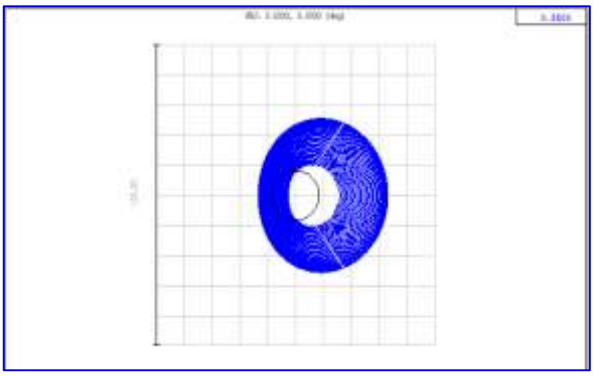

(F)

Figure 2. Spot diagram at various incidence angles in the case of the secondary mirror attached to the lens which is (A,B,C,D,E,F) represents the angles (0,0.1,0.2,0.3,0.4,0.5) respectively.

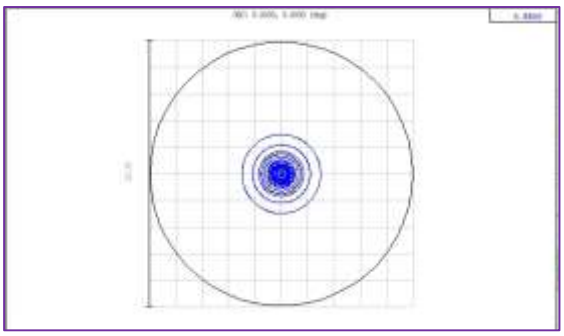

(A)

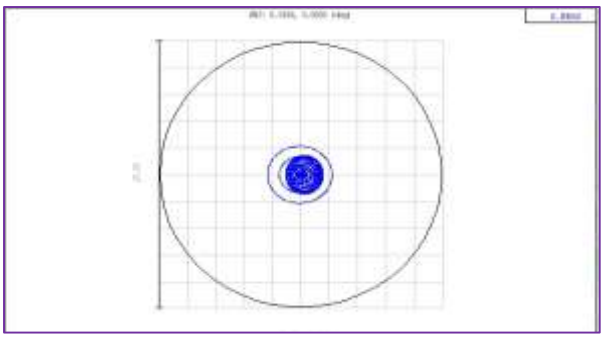

(B)

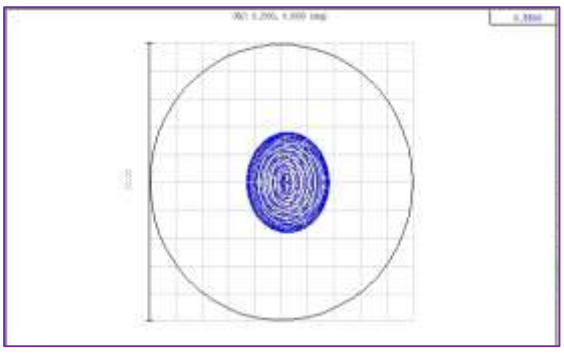

(C)

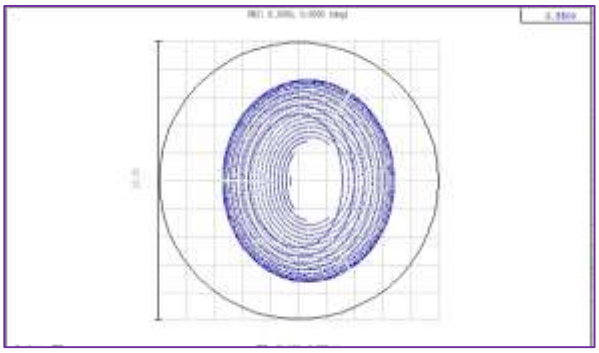

(D)

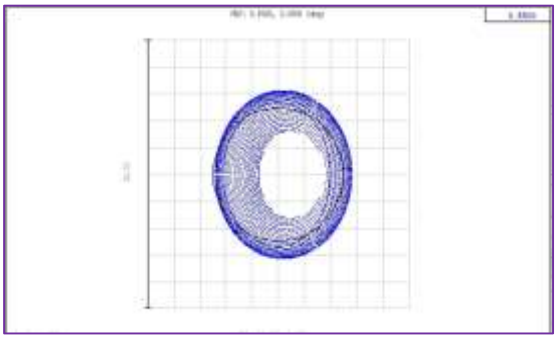

(E)

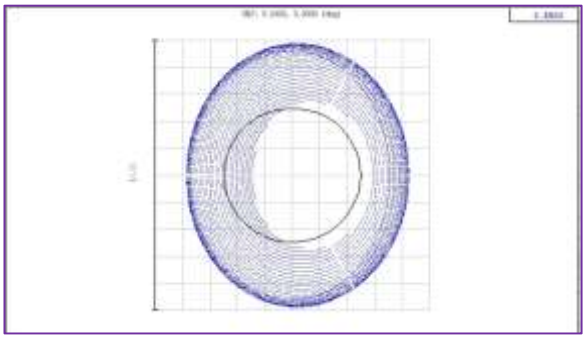

(F)

Figure 3. Spot diagram at various incidence angles in the case of the lens nonattached to the secondary mirror lens which is (A,B,C,D,E,F) represents the angles (0,0.1,0.2,0.3,0.4,0.5) respectively.

.

4.2. Point Spread Function (PSF)

The point spread function curve is what provides the two-dimensional intensity distribution in the image plane. In the first design, we see in figure 4 that there are several pretty high peaks on the surface of the image at the angle of incidence (0, 0.1). Since the shape is regular, the point spread function indicates that there isn't an aberration. In terms of the angles (0.2, 0.3, 0.4, and 0.5), we observe a gradual loss in intensity and the appearance of elevations on both sides of the picture. Due to the aberration, the intensity distribution in the image plane is unbalanced.

In the second design, at the angles (0, 0.1, 0.2, 0.3), we observe in Figure 5 that there are several high peaks free from aberration. We notice a little decrease in the intensity when the angles are gradually increased due to the presence of aberration.

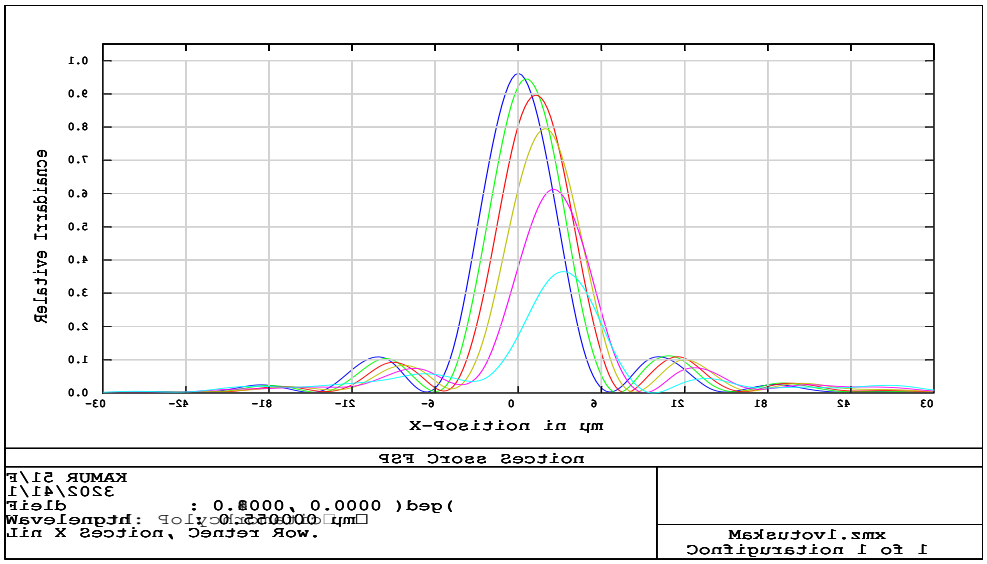

Figure 4. PSF at various incidence angles in the case of the secondary mirror attached to the lens.

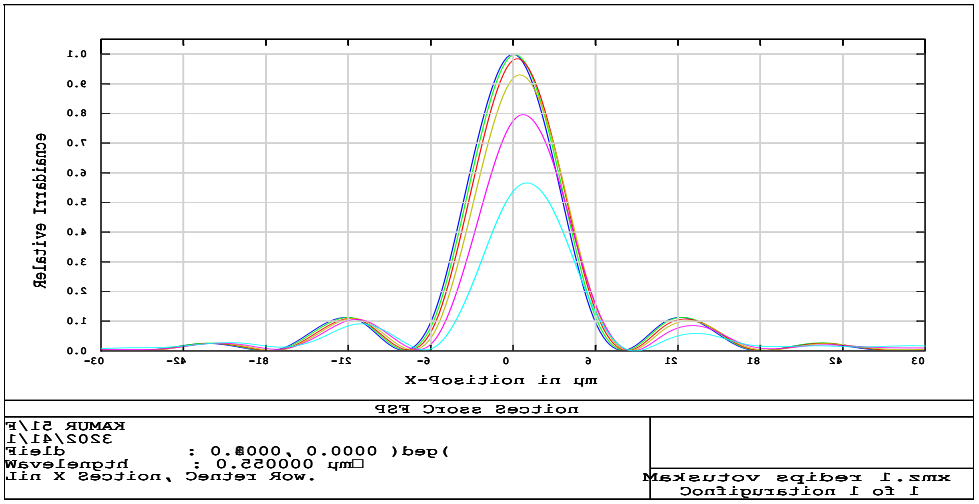

Figure 5. PSF at various incidence angles in the case of the lens nonattached to the secondary mirror.

4.3. Modulation Transfer Function (MTF)

Regarding the optical transition mechanism based on **Figure 6**, the sagittal axis and tangential axis of the optical transition function curve change as the angles of incidence of rays change. Because of symmetry, the function curves for the sagittal and tangential axes are identical at the angle of incidence (0°). The tangential and sagittal axes of the remaining angles (0.1, 0.2, 0.3, 0.4, and 0.5)

contain two curves, which show how the loss of symmetry has changed the value of the function for the two axes. The function curve for the sagittal and tangential axes diverges more as the angle of incidence increases.

As for the modulation transmission function in the case of the secondary mirror not attached to the correction lens, the function curves of the sagittal and tangential axes are identical in the angles of incidence (0, 0.1, and 0.2). The transverse and sagittal axes of the remaining angles (0.3, 0.4, and 0.5) contain two curves. The function curve of the sagittal and tangential axes diverges more as the angle of incidence increases, and we notice the polychromatic diffraction MTF curve in **Figure (7)** is approximately identical to the diffraction limit (the curve in black color).

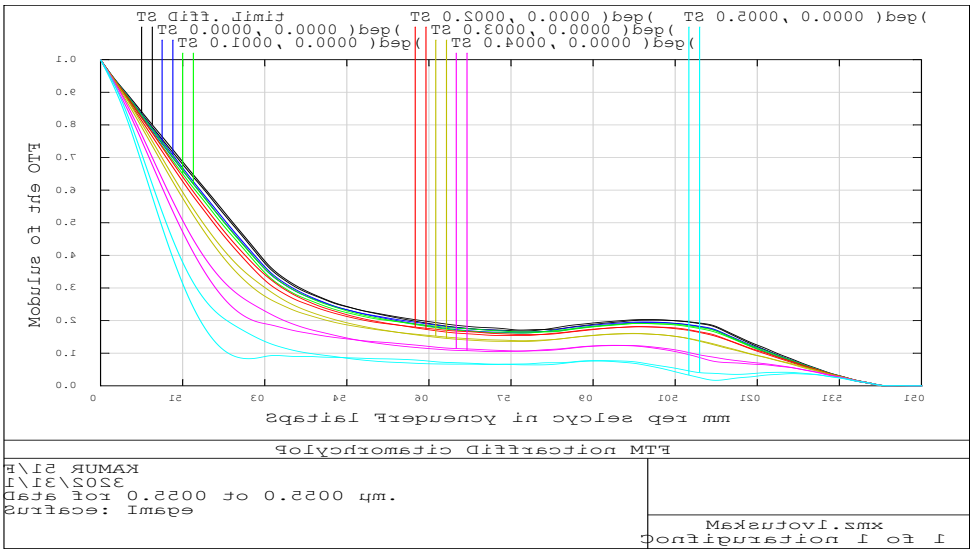

Figure 6. MTF diagram at various incidence angles in the case of the secondary mirror attached to the lens.

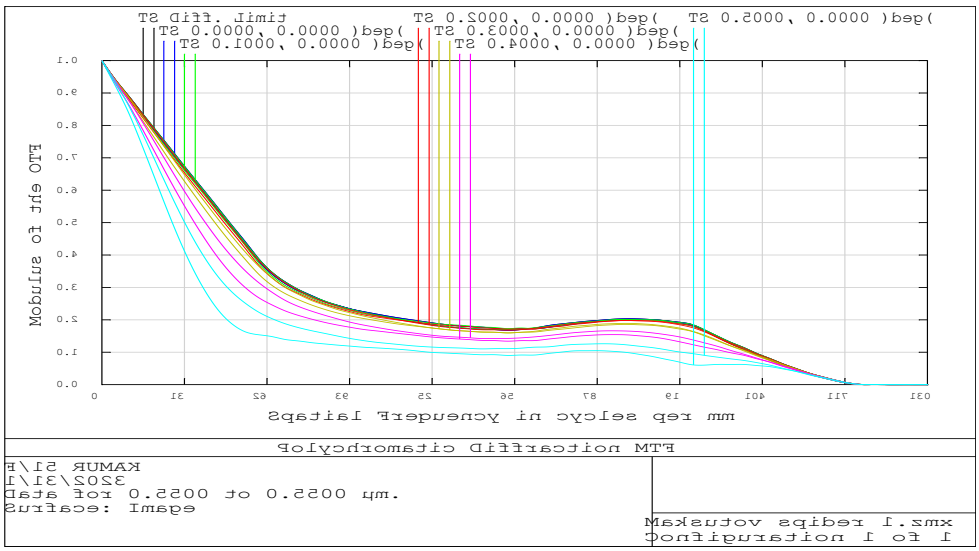

Figure 7. MTF diagram at various incidence angles in the case of the lens nonattached to the secondary mirror.

4.4. Optical Path Difference (OPD)

In the first case, we notice from **Figure 8** the difference in the optical path with respect to the angles of incidence (0.1, 0.2, 0.3, 0.4, 0.5). We note that the optical path difference appears in a small amount at the angle (0.1, 0.2, 0), and the curve increases with an increase in angle value each time. The optical path divergence pattern in this case is asymmetric due to the asymmetry in the incidence of rays on the optical system.

In the second case, we notice that the optical path difference appears in a small amount at the angle (0.3, 0.1, 0.2, 0) in the **Figure (9)**, and the curve increases with an increase in the value of the angle at (0.4, 0.5).

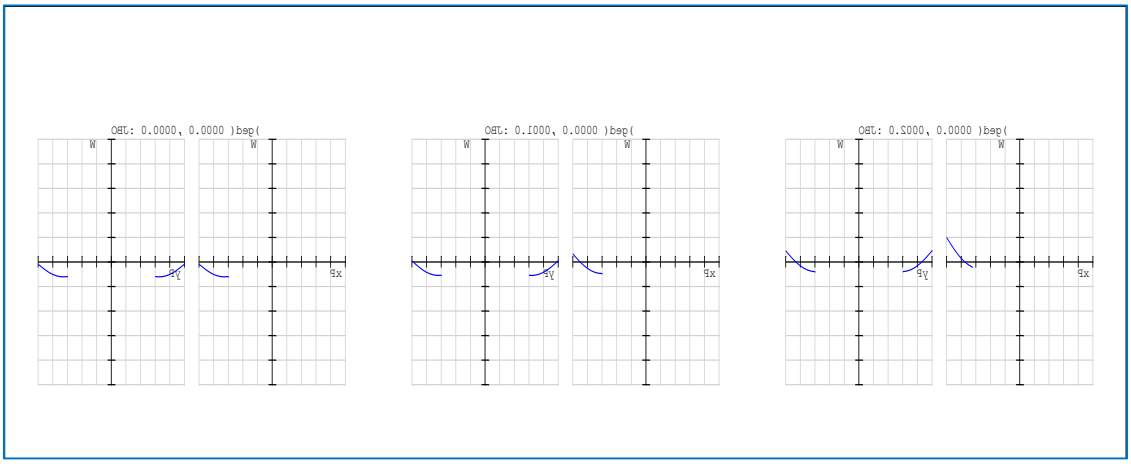

(A)

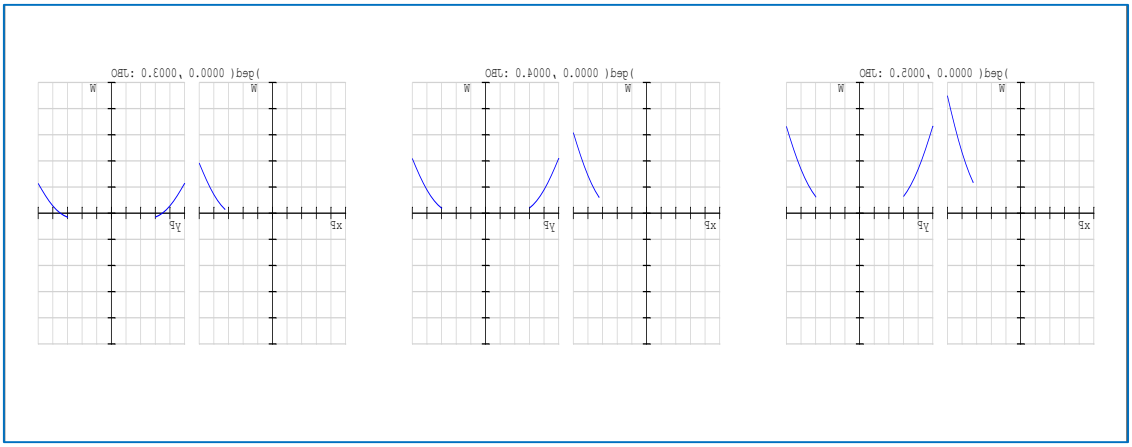

(B)

Figure 8. OPD diagram at various incidence angles in the case of the secondary mirror attached to the lens which is (A) represents the angles (0,0.1,0.2) and (B) represents the angles 0.3,0.4,0.5) respectively .

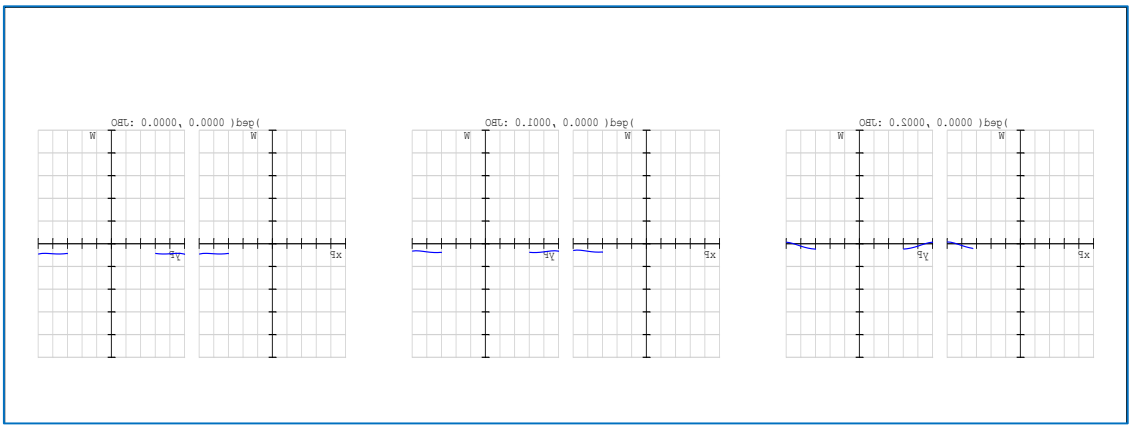

(A)

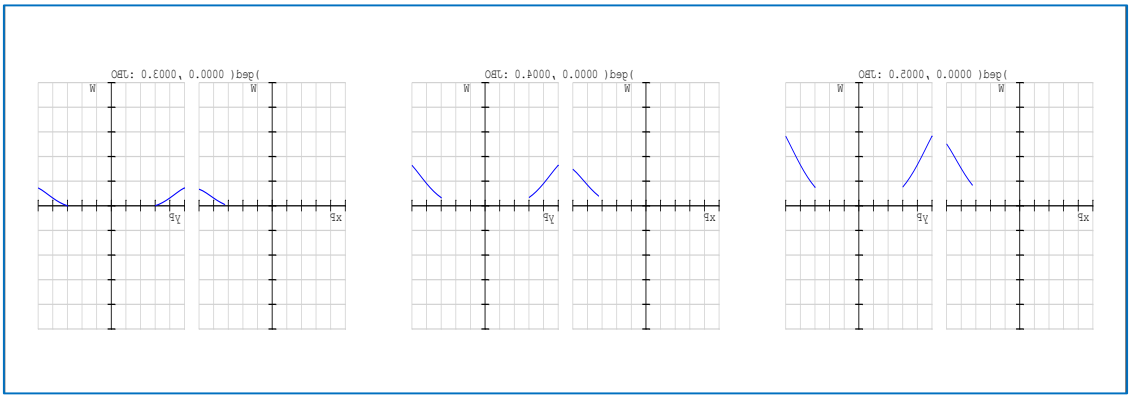

(B)

Figure 9. OPD diagram at various incidence angles in the case of the lens nonattached to the secondary mirror which is (A) represents the angles (0,0.1,0.2) and (B) represents the angles (0.3,0.4,0.5) respectively .

4.5. Ray Fan Aberration

You can see how the shape of the aberration curve changes as the angle of incidence of the rays changes. This is because the asymmetrical aberration value goes up. The ray aberration curves for different angles of incidence show this.

In the first design, the aberration curve for angles of incidence (0, 0.1, 0.2, 0.3, 0.4, and 0.5) is shown in Figure 10. We see that the aberration curve steadily steepens and deviates from the horizontal axis as the value of the angle of incidence increases (which is the image quality criterion for this scheme; the closer the curve is to the horizontal axis, the less aberration will be).

In **Figure 11**, the aberration curve is shown for the angles of incidence (0, 0.1, 0.2, and 0.3) close to the horizontal axis for the second design. As for the angles of incidence (0.4 and 0.5), we see that the deviation curve is steeper and deviates from the horizontal axis.

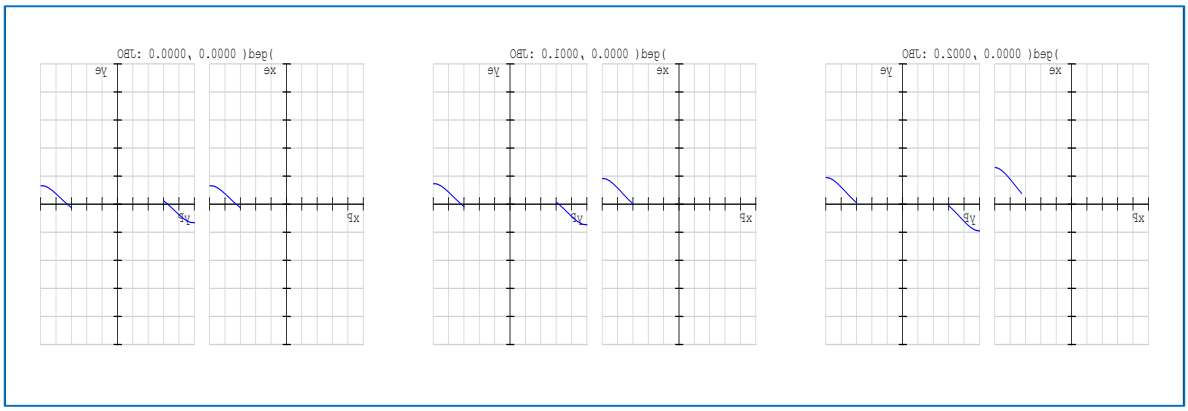

(A)

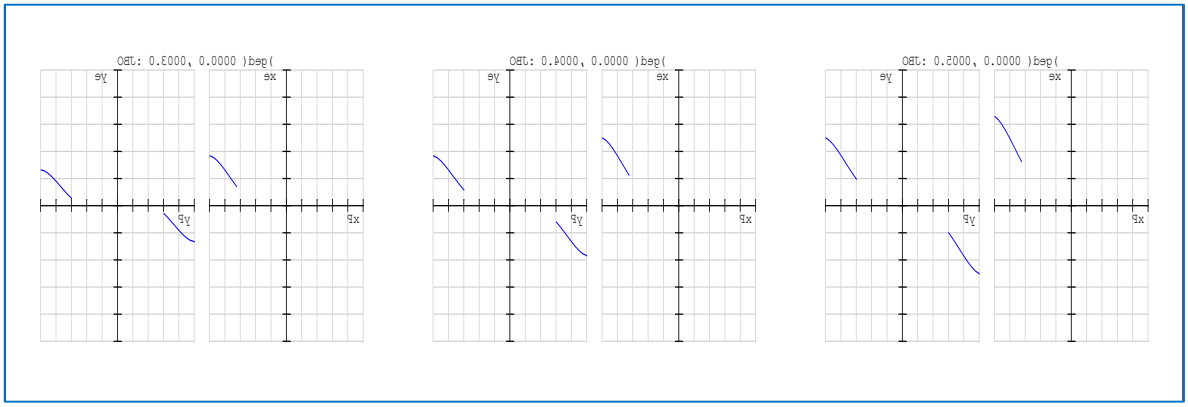

(B)

Figure 10. RFA diagram at various incidence angles in the case of the secondary mirror attached to the lens which is (A) represents the angles (0,0.1,0.2) and (B) represents the angles 0.3,0.4,0.5) respectively .

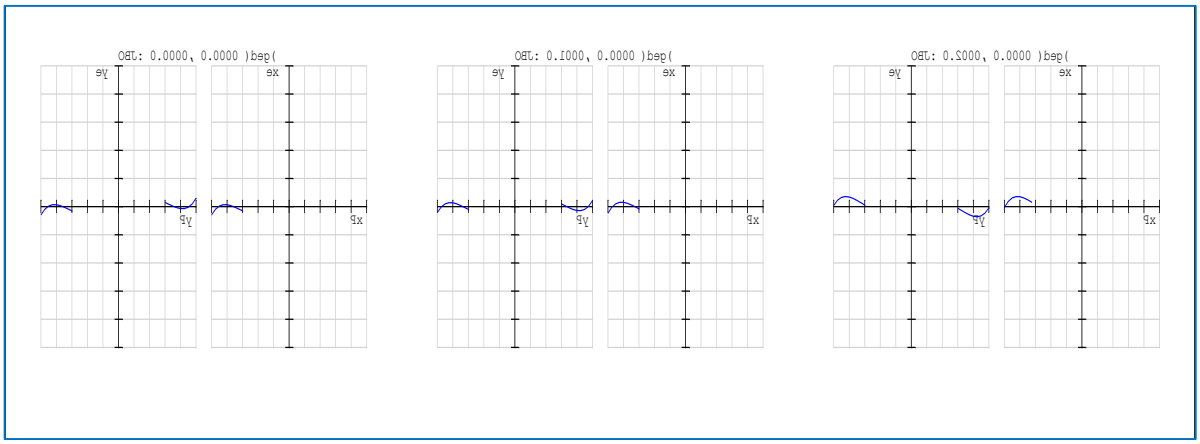

(A)

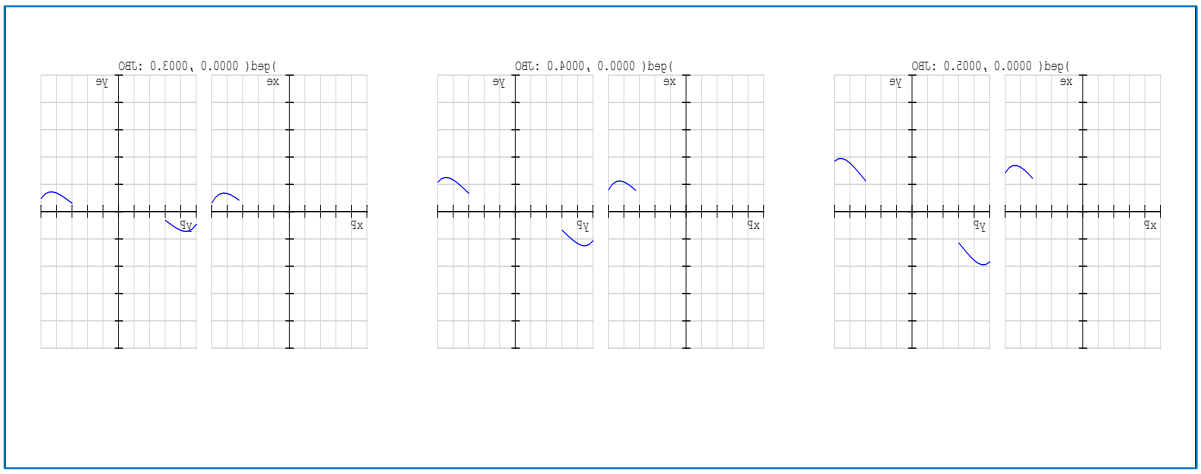

(B)

Figure 11. RFA diagram at various incidence angles in the case of the lens nonattached to the secondary mirror which is (A) represents the angles (0,0.1,0.2) and (B) represents the angles 0.3,0.4,0.5) respectively .

4.6.Encircled Energy

The accumulated energy curve symmetrically depicts the distribution of light energy on the image plane, from the center out to the edges. where the energy begins at zero at the picture plane's center and steadily rises as the radius of the cross section of the image plane increases. The value of the accumulated energy after that is constant regardless of how much the radius of the cross-sectional circle for the picture plane increases because the energy is distributed solely inside until it reaches its peak when covering the area for all of the stored energy.

Regarding the energy gathered when the beams' angle of incidence shifts, with a greater angle of incidence, the stored energy seems to cover more space in the image plane. That is, the expansion of the image plane's special area segments, as shown in the **Figures (12, 13)**.

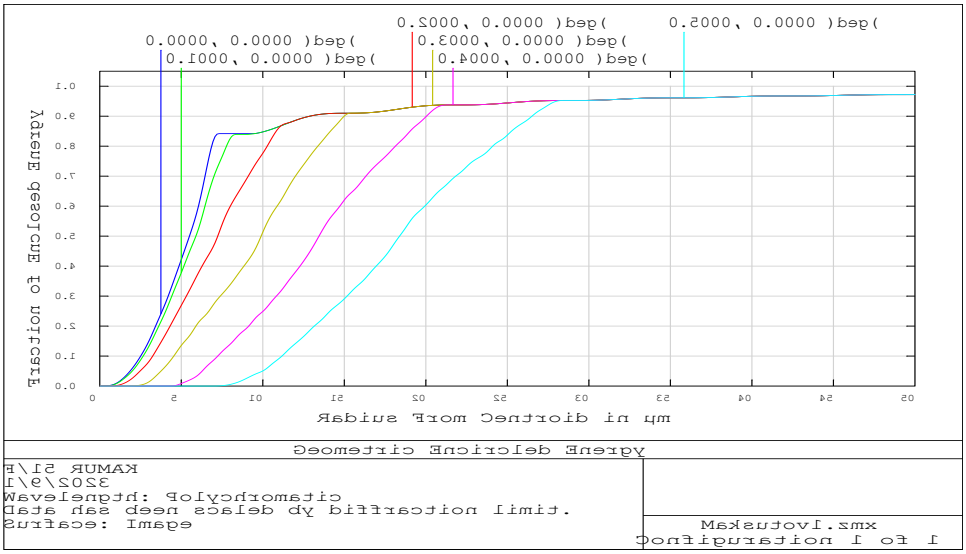

Figure 12. Enc diagram at various incidence angles in the case of the secondary mirror attached to the lens.

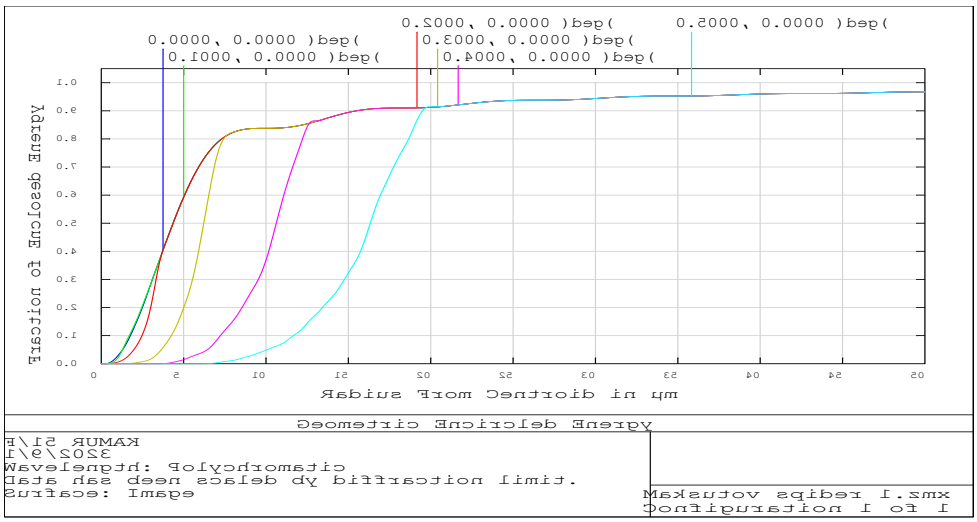

Figure 13. Enc diagram at various incidence angles in the case of the lens nonattached to the secondary mirror.

5. Conclusion

The two models of the Cassegrain telescope had a correction lens that eliminated image error caused by aberration, but they differed in the location of the lens. The results obtained from the research showed the quality of the image when the secondary mirror is not attached to the correction lens; it gives a clear image compared to the telescope whose secondary mirrors are attached to the correction lens and the telescope whose correction lens is located between the two mirrors. In the first design, the tangential and sagittal axes in the MTF function of the remaining angles (0.1, 0.2, 0.3, 0.4, and 0.5) contain two curves, which show how the loss of symmetry has changed the value of the function for the two axes. In the second design, the sagittal and tangential axes are identical in the angles of incidence (0, 0.1, and 0.2), and the transverse and sagittal axes of the remaining angles (0.3, 0.4, and 0.5) contain two curves. The analysis tools used in the research gave a clear idea of the performance of the optical system represented by the telescope by evaluating the image quality through the criteria used in these tools. In PSF for the first design, there are several pretty high peaks on the surface of the image at the angle of incidence (0, 0.1). Since the shape is regular, the point spread function indicates that there isn't an aberration, but in terms of the angles (0.2, 0.3, 0.4, 0.5), we observe a gradual loss in intensity and the appearance of elevations on both sides of the picture. In the second design, at the angles (0, 0.1, 0.2, 0.3), we observe in **Figure 5** that there are several high peaks free from aberration.

Acknowledgement

I extend my thanks to the College of Education for pure science Ibn Al-Haitham, University of Baghdad for providing assistance to complete this work by opening private laboratories and providing scientific facilities by the staff of the Physics Department to help support the research project.

Conflict of Interest

The authors declare that they have no conflicts of interest

Funding: None.

References

1. Katz, M.; Introduction to geometrical optics, *World Scientific Publishing Co. Pte. Ltd. Singapore* **2002,** *23*, 23-34.
2. Maksutov, D. D.; *Newcatadioptric meniscus system, JOSA*, **1984,** 34. 270.
3. Kinzer, P. E.; Stargazing Basics Getting Started in Recreational Astronomy, *Cambridge University Press* . **2015**, *12*, 43-55.
4. Mullaney, J.; *A Buyer's and User's Guide to Astronomical Telescopes & Binoculars*. **2007**, 46. ISBN 9781846287077.
5. Baril, M. R.; A photovisual Maksutov Cassegrain telescope". Although convenient, this design is limited to focal ratios above *f*/15 unless an aspheric correction is applied to some element in the optical system. **2005**, *34*, 55-67.
6. Gross, H.; Fritz, B.; Bertram, A.; Telescopes. Handbook of Optical Systems*: Survey of Optical Instruments* . **2008,** *4*, 723-864.
7. H. Y.; Al Hammod, Design And Analysisa Zoom Cassegrain Telescope Cover Middle Ir Region Using Zemax Program, **2017,** *6, 8*, 178–185.
8. Kamus, S. F.; Lipin, N. A.; Sokolskii, M. N.; Levandovskaya, L. E.; Denisenko, S. A. Amateur telescopes, *J. Opt. Technol*. **2002**, *69*, 671-688
9. Shwayyea, A. K.; Hasan, A. B. Simulation and Evaluation of a Variable Effective Focal Length of Refractive Binocular Telescope. *Ibn Al-Haitham Journal for Pure and Applied Sciences.* **2022,** *35*,*3*, 65-75.
10. Mullaney, J.; A Buyer's and User's Guide to Astronomical Telescopes and Binoculars. *Springer*. **2007,** *33*, 56-76 .
11. *Baril, M. R.;*. A photovisual Maksutov Cassegrain telescope. *Archived from* the original. **2006,** *10*, 29-38.
12. Karp, J.International Telecommunication Union (ITU), *Optical System design and Engineering Consideration*, **2016,** *12*, 78- 88.
13. K.; Miyamoto, Image Evaluation by Spot Diagram Using A Computer, *Appl. Opt.* **1963**, *2*, 1247-1250.
14. H.; Zuo, F. H.; Nia, S.; He, Soi MUMPs Micro mirror Scanner and its Application in Laser line Generator, Journal of Micro /Nanolithography ,MEMS and MOEMS , **2017,** *16,1*, 45-66.
15. Braat, J. M.; Assessment of optical systems by means of point-spread functions. *Progress in optics* **2008,** *51*, 349-468.
16. Liou, H.; Brennan, N.; Anatomically accurate, finite model eye for optical modeling. *J. Opt. Soc. Am*. **1997,** *14 ,8*, 1684–1695.
17. Thoeniss, T.; Gerhard, C.; Adam, G.; Optical system design, *Jornal of Opt.* **2009,** *45, 2*, 55-67
18. Hsu, M. Y.; Shenq,T. C.; Ting, M. H.; Thermal optical path difference analysis of the telescope correct lens assembly. *Advanced Optical Technologies*. **2012,** *1, 6*,447-453.
19. Mahajan , V. N.; Optical Imaging and Aberrations :Ray Geometrical Optics ,Part I,II , *SPIE Press Monograph*, **1998,** 45, 12- 34.
20. Sanyal, S.; Ajay, G.; The factor of encircled energy from the optical transfer function. *Journal of Optics A: Pure and Applied Optics*. **2002,** *4, 2*,208-213.
21. Al-Saadi, T. M.; Hussein, B. H.; Hasan, A. B.; Shehab. A. A.; Study the structural and optical properties of Cr doped SnO_2 nanoparticles synthesized by sol-gel method. *Energy Procedia*. **2019**, *157*, 457–465.
22. A. B.; Hasan, S. A.; Husain, Design of Light Trapping Solar Cell System by Using Zemax Program. *Journal of Physics: Conference Series*. **2018,** *1003*, 25- 32.

23. Hasan, A. B.Studying Optical Properties of Quantum Dot Cylindrical Fresnel Lens. *NeuroQuantology,* **2022,** *20*, 97–104.
24. Hamza, H. N.; Hasan, A. B.Design of Truncated Hyperboloid Solar Concentrator by Using Zemax Program. *Ibn Al-Haitham Jour. for Pure & Appl. Sci*. **2022,** *35,1*, 1-7.
25. Al-Hamdani, A. H.; Rashid, H. G.; Hasan, A. B. Irradiance distribution of image surface in microlens array solar concentrator. *ARPN Journal of Engineering and Applied Sciences*, **2013**, *5*, 23-31.
26. Karszewski, K. M.; Stewen, C.; Giesen A.; Huge, H.; Theoretical modeling and experimental investigations of the diode-pumped thin-disk Yb :YAG laser, Quantum Electron **1999** , *29* , *8* ,697.
27. Mohammad, H. S.Determination and suppression of back reflected pump power in Yb:YAG thin-disk laser , *Optical Engineer* **2017** ,*56(2)*, 026109-1-8.
28. Hariton, V.; Feasibility study and simulation of a high energy diode pumped solid-state amplifier ,*Tecnico Lisboa*. **2016** ,1-94.
29. Kazemi, S. S., Mahdieh, M. H.; Determination and suppression of back-reflected pump power in Yb:YAG thin-disk laser, *Optical Engineering* **2017**,*56(2)*,026109.doi: 10.1117/1.oe.56.2.026109.
30. Weichelt, V.; Von, B.; Experimental Investigations on Power Scaling of High-Brightness cw Ytterbium-Doped Thin-Disk Lasers, (July) **2021**,1–23.